

Article

Peristaltic Blood Flow of Couple Stress Fluid Suspended with Nanoparticles under the Influence of Chemical Reaction and Activation Energy

Rahmat Ellahi ^{1,2,*} , Ahmed Zeeshan ² , Farooq Hussain ^{2,3} and A. Asadollahi ⁴

¹ Center for Modeling & Computer Simulation, Research Institute, King Fahd University of Petroleum & Minerals, Dhahran 31261, Saudi Arabia

² Department of Mathematics & Statistics, FBAS, IIUI, Islamabad 44000, Pakistan; ahmad.zeeshan@iiu.edu.pk (A.Z.); farooq.hussain@buitms.edu.pk (F.H.)

³ Department of Mathematics, (FABS), BUIITEMS, Quetta 87300, Pakistan

⁴ Department of Mechanical Engineering & Energy Processes, Southern Illinois University, Carbondale, IL 62901, USA; arash.asadollahi@siu.edu

* Correspondence: rellahi@alumni.ucr.edu

Received: 28 January 2019; Accepted: 19 February 2019; Published: 21 February 2019



Abstract: The present study gives a remedy for the malign tissues, cells, or clogged arteries of the heart by means of permeating a slim tube (i.e., catheter) in the body. The tiny size gold particles drift in free space of catheters having flexible walls with couple stress fluid. To improve the efficiency of curing and speed up the process, activation energy has been added to the process. The modified Arrhenius function and Buongiorno model, respectively, moderate the inclusion of activation energy and nanoparticles of gold. The effects of chemical reaction and activation energy on peristaltic transport of nanofluids are also taken into account. It is found that the golden particles encapsulate large molecules to transport essential drugs efficiently to the effected part of the organ.

Keywords: chemical reaction; activation energy; peristalsis; couple stress fluid; nanoparticle; Keller-box method

1. Introduction

In any living organism peristaltic motion is mainly caused by the contraction and expansion of some flexible organs. This applies a pressure force to drive fluids, for example, blood in veins, urine to bladder, and transport of medicines to desired locations are a few common biological examples. The rapid developments in nano-science have noticeably revolutionized almost every field of life, particularly in medical sciences. The advent of nano-technology in medicines has brought miraculous changes by reshaping the primitive methods of treatment. Nowadays, in developed countries operations are preferably performed without involving any prunes and cuts, which was once thought to be very complex and menacing for cancer treatment, brain tumors, lithotripsy, etc. Regardless of many other uses of nanofluids in industrial and practical settings, the primary objective of nanoparticles is the enhancement of heat transfer [1]. It is mainly due to their high conductivity. In addition to the size and type of nanoparticles, other factors, such as temperature, volume fraction, and thermal conductivity are also very important to maximize the thermal conductivity. In pursuit of attaining such enhancement in the system, with the passage of time many useful models based on the physical properties of the matter have been developed. On the said topic, scholars have made full use of these models in their analyses, experiments, and conditions, which have been discussed here very briefly. For instance, the investigation of Tripathi and Beg [2] explains the application of peristaltic micropumps and novel drug delivery systems in pharmacological engineering. They formulated

their study with the help of the Buongiorno nanofluid model and treated blood as Newtonian fluid. El-dabe et al. [3] have explained the significant contribution of nanofluids in peristalsis. They produced their results for flexible wall properties, lubrication, MHD, and porosity. As generally it is believed that the motion of blood is likely to be non-Newtonian, therefore, Swarnalathamma and Krishana [4] have studied the physiological flow of the blood in the micro circulatory system by taking account of the particle size effect. They considered couple stress fluid for the given peristaltic analysis, which is further affected by magnetic fields. The effects of channel inclination are studied by Shit and Roy [5]. The couple stress fluid influenced by constant application of magnetic fields is used as the base fluid. Jamalabad et al. [6] reported the effects of biomagnetic blood flow through a stenosis artery by means of non-Newtonian flow of a Carreau-Yasuda fluid model. They carried out a numerical simulation of an unsteady blood flow problem. Hosseini et al. [7] have presented the thermal conductivity of a nanofluid model. To perform this investigation, the nanofluid model is considered as the function of thermal conductivity of nanoparticles, base fluid, and interfacial shell properties by considering temperature as the most effective of parameters involved in the study. The most noteworthy contributions on the matter can be seen in the list of references [8–19]. Furthermore, activation energy has a key role in industries, in particular, effectively aggravating slow chemical reactions in chemistry laboratories to improve the efficiency of various mechanisms by adding activation energy to respective physical and mechanical processes. Mustafa et al. [20] have proposed a chemical and activation energy MHD-affected mix convection flow of nanofluids. In this study the flow over the vertical sheet expands due to high temperature and causes the fluid motion is analyzed numerically. A few of the latest works related to this present work have been listed in [21–28].

In view of the existing literature, one can feel the application of nanotechnology in medical science opens a new dimension for researchers to turn their attention towards the effective role of chemical reaction and activation energy [29–31], since nanoparticles help in treating different diseases by means of the peristaltic movement of blood. Such biological transport of blood helps to deliver drugs or medicine effectively to the damaged tissue or organ. As a matter of fact, this effort is devoted to inspecting the simultaneous effects of chemical reaction and activation energy for the peristaltic flow of couple stress nanofluids in a single model, which is yet not available in literature, and could have dual applications in expediting the treatment process.

2. Formulism

The inner tube is of a rigid configuration, while the outer tube is flexible in nature as shown in Figure 1. The sinusoidal waves travel with a constant speed through its walls, due to the stress caused by an unsteady movement of heated nanofluid through the space between both tubes. The general form of equations governing the two-dimensional flows are given as:

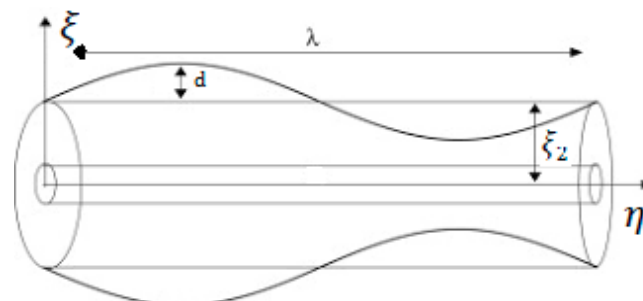


Figure 1. Configuration of coaxial tubes.

Conservation of mass

$$\nabla \cdot \vec{V} = 0. \quad (1)$$

Conservation of momentum

$$\rho_f \left(\vec{V} \cdot \vec{\nabla} \right) \vec{V} = -\vec{\nabla} P^* + \mu \nabla^2 \vec{V} + \left[\varphi \rho_p + (1 - \varphi) \left\{ \rho_f (1 - \beta_T (v - v_w)) \right\} \right] g - \gamma_1 \nabla^4 \vec{V}. \quad (2)$$

Thermal energy

$$(\rho c)_f \left(\vec{V} \cdot \vec{\nabla} \right) v = k \nabla^2 v + (\rho c)_p \left[D_b \vec{\nabla} \varphi \cdot \vec{\nabla} v + \frac{D_T}{v_w} \vec{\nabla} v \cdot \vec{\nabla} v \right]. \quad (3)$$

Concentration of nanoparticles

$$\rho_p \left(\vec{V} \cdot \vec{\nabla} \right) \varphi = D_b \nabla^2 \varphi + \frac{D_T}{v_w} \nabla^2 v - k_r^2 \left(\frac{v}{v_w} \right)^n (\varphi - \varphi_w) \exp \left(\frac{-E_a}{kv} \right). \quad (4)$$

One can easily identify that the last term in the momentum equation describes the velocity of couple stress fluid involving a constant associated with the couple stress fluid γ_1 . The last term in Equation (4) on the right side is known as “Arrhenius term”, which shows the effects of chemical reaction and activation energy incorporated to a nanofluid. The radial and axial velocity components of nanofluids are respectively defined by $u(\xi, \eta)$ and $w(\xi, \eta)$ in two concentric tubes, such that there is no rotation about their axes. A peristaltic flow of a heated couple stress fluid carrying the gold nanoparticles (GNPs) through these coaxial tubes due to the contraction and expansion of flexible walls of the outer tube is assumed. If the two-dimensional peristaltic motion of the concerned nanofluid is denoted by $[u(\xi, \eta) \ 0 \ w(\xi, \eta)]$, then the Equations (1)–(4) in the component’s form will take the following form:

$$\frac{u}{\xi} + \frac{\partial u}{\partial \xi} + \frac{\partial w}{\partial \eta} = 0, \quad (5)$$

$$\begin{aligned} \rho_f \left(\frac{\partial u}{\partial t} + u \frac{\partial u}{\partial \xi} + w \frac{\partial u}{\partial \eta} \right) &= -\gamma_1 \left[\frac{\partial^4 u}{\partial \xi^4} + \frac{\partial^4 u}{\partial \eta^4} + \frac{\partial^4 u}{\partial \xi^2 \partial \eta^2} + \frac{\partial^4 u}{\partial \eta^2 \partial \xi^2} + 2 \frac{\partial^3 u}{\xi \partial \xi^3} + \frac{\partial^3 u}{\xi \partial \xi \partial \eta^2} + \frac{\partial^3 u}{\xi \partial \eta^2 \partial \xi} \right. \\ &\quad \left. + \frac{\partial^2 u}{\xi^2 \partial \xi^2} + \frac{\partial u}{\xi^3 \partial \xi} \right] - \frac{\partial P}{\partial \xi} + \mu \left(\frac{\partial^2 u}{\partial \xi^2} + \frac{\partial u}{\xi \partial \xi} + \frac{\partial^2 u}{\partial \eta^2} \right), \end{aligned} \quad (6)$$

$$\begin{aligned} \rho_f \left(\frac{\partial w}{\partial t} + u \frac{\partial w}{\partial \xi} + w \frac{\partial w}{\partial \eta} \right) &= -\gamma_1 \left[\frac{\partial^4 w}{\partial \xi^4} + \frac{\partial^4 w}{\partial \eta^4} + \frac{\partial^4 w}{\partial \xi^2 \partial \eta^2} + \frac{\partial^4 w}{\partial \eta^2 \partial \xi^2} + \frac{\partial^3 w}{\xi \partial \xi^3} + \frac{\partial^3 w}{\xi \partial \xi \partial \eta^2} + \frac{\partial^3 w}{\xi \partial \eta^2 \partial \xi} \right. \\ &\quad \left. - \frac{\partial^2 w}{\xi^2 \partial \xi^2} + \frac{\partial w}{\xi^3 \partial \xi} \right] + \left[\varphi \rho_p + (1 - \varphi) \left\{ \rho_f (1 - \beta_T (v - v_w)) \right\} \right] g - \frac{\partial P}{\partial \eta} \\ &\quad + \mu \left(\frac{\partial^2 w}{\partial \xi^2} + \frac{1}{\xi} \frac{\partial w}{\partial \xi} + \frac{\partial^2 w}{\partial \eta^2} \right), \end{aligned} \quad (7)$$

$$\begin{aligned} (\rho c)_f \left(\frac{\partial v}{\partial t} + u \frac{\partial v}{\partial \xi} + w \frac{\partial v}{\partial \eta} \right) &= (\rho c)_p \left[D_b \left\{ \frac{\partial \varphi}{\partial \xi} \frac{\partial v}{\partial \xi} + \frac{\partial \varphi}{\partial \eta} \frac{\partial v}{\partial \eta} \right\} + \frac{D_T}{v_w} \left\{ \left(\frac{\partial v}{\partial \xi} \right)^2 + \left(\frac{\partial \varphi}{\partial \eta} \right)^2 \right\} \right] \\ &\quad + k \left(\frac{\partial^2 v}{\partial \xi^2} + \frac{1}{\xi} \frac{\partial v}{\partial \xi} + \frac{\partial^2 v}{\partial \eta^2} \right), \end{aligned} \quad (8)$$

$$\begin{aligned} \left(\frac{\partial \varphi}{\partial t} + u \frac{\partial \varphi}{\partial \xi} + w \frac{\partial \varphi}{\partial \eta} \right) &= D_b \left(\frac{\partial^2 \varphi}{\partial \xi^2} + \frac{1}{\xi} \frac{\partial \varphi}{\partial \xi} + \frac{\partial^2 \varphi}{\partial \eta^2} \right) + \frac{D_T}{v_w} \left(\frac{\partial^2 v}{\partial \xi^2} + \frac{1}{\xi} \frac{\partial v}{\partial \xi} + \frac{\partial^2 v}{\partial \eta^2} \right) \\ &\quad - k_r^2 \left(\frac{v}{v_w} \right)^n (\varphi - \varphi_w) \exp \left(\frac{-E_a}{kv} \right). \end{aligned} \quad (9)$$

The corresponding boundary at the extreme wall.

At the rigid wall:

$$\left. \begin{aligned} (i). \ w(\xi) &= 0, \\ (ii). \ v(\xi) &= v_m, \\ (iii). \ \varphi(\xi) &= \varphi_m. \end{aligned} \right\}; \text{ When } \xi = \xi_1. \quad (10)$$

At the flexible wall:

$$\left. \begin{array}{l} (i). w(\xi) = 0, \\ (ii). v(\xi) = v_w, \\ (iii). \varphi(\xi) = \varphi_w. \end{array} \right\}; \text{ When } \xi = \xi_2. \quad (11)$$

As the unsteady peristaltic flow of nanofluids in the laboratory frame (ξ, η) is considered, thus a wave frame (ξ^*, η^*) , which moves corresponding to the wave that travels on the flexible and parallel walls of the outer tube, is taken into account. Let “ c ” be the constant velocity of the wave frame, such that:

$$\begin{aligned} \xi^* &= \xi; & \eta^* &= \eta - ct; & u^* &= u; & w^* &= w - c; \\ v^*(\xi^*, \eta^*) &= v(\xi, \eta, t); & \varphi^*(\xi^*, \eta^*) &= \varphi(\xi, \eta, t). \end{aligned} \quad (12)$$

In view of the transformation given in Equation (10), the governing Equations (6)–(9) in wave frame can be written as:

$$\begin{aligned} \rho_f \left[\left(\frac{-\delta c^2}{\lambda} \right) \frac{\partial \bar{u}}{\partial \eta} + \left(\frac{\delta^2 c^2}{\xi^2} \right) \bar{u} \frac{\partial \bar{u}}{\partial \xi} + \left(\frac{\delta c^2}{\lambda} \right) \bar{w} \frac{\partial \bar{u}}{\partial \eta} \right] \\ = -\gamma_1 \left[\left(\frac{\delta c}{\xi^2} \right) \frac{\partial^4 \bar{u}}{\partial \xi^4} + \left(\frac{\delta c}{\lambda^4} \right) \frac{\partial^4 \bar{u}}{\partial \eta^4} + \left(\frac{\delta c}{\lambda^2 \xi^2} \right) \frac{\partial^4 \bar{u}}{\partial \xi^2 \partial \eta^2} + \left(\frac{\delta c}{\lambda^2 \xi^2} \right) \frac{\partial^4 \bar{u}}{\partial \eta^2 \partial \xi^2} \right. \\ \left. + \left(\frac{2\delta c}{\xi^4} \right) \frac{\partial^3 \bar{u}}{\xi \partial \xi^3} + \left(\frac{\delta c}{\lambda^2 \xi^2} \right) \frac{\partial^3 \bar{u}}{\xi \partial \xi \partial \eta^2} + \left(\frac{\delta c}{\lambda^2 \xi^2} \right) \frac{\partial^3 \bar{u}}{\xi \partial \eta^2 \partial \xi} + \left(\frac{\delta c}{\xi^4} \right) \frac{\partial^2 \bar{u}}{\xi^2 \partial \xi^2} \right. \\ \left. + \left(\frac{\delta c}{\xi^4} \right) \frac{\partial^2 \bar{u}}{\xi^3 \partial \xi} \right] - \left(\frac{\mu \lambda c}{\xi^2} \right) \frac{\partial \bar{P}}{\partial \xi} + \mu \left[\left(\frac{\delta c}{\xi^2} \right) \frac{\partial^2 \bar{u}}{\partial \xi^2} + \left(\frac{\delta c}{\xi^2} \right) \frac{\partial \bar{u}}{\xi \partial \xi} + \left(\frac{\delta c}{\lambda^2} \right) \frac{\partial^2 \bar{u}}{\partial \eta^2} \right], \end{aligned} \quad (13)$$

$$\begin{aligned} \rho_f \left[-c \frac{\partial(w^*+c)}{\partial \eta^*} + u^* \frac{\partial(w^*+c)}{\partial \xi^*} + (w^*+c) \frac{\partial(w^*+c)}{\partial \eta^*} \right] \\ = -\gamma_1 \left[\frac{\partial^4(w^*+c)}{\partial \xi^{*4}} + \frac{\partial^4(w^*+c)}{\partial \eta^{*4}} + \frac{\partial^4(w^*+c)}{\partial \xi^{*2} \partial \eta^{*2}} + \frac{\partial^4(w^*+c)}{\partial \eta^{*2} \partial \xi^{*2}} \right. \\ \left. + \frac{2\partial^3(w^*+c)}{\xi^* \partial \xi^{*3}} + \frac{\partial^3(w^*+c)}{\xi^* \partial \xi^* \partial \eta^{*2}} + \frac{\partial^3(w^*+c)}{\xi^* \partial \eta^{*2} \partial \xi^*} + \frac{\partial^2(w^*+c)}{\xi^{*2} \partial \xi^{*2}} \right. \\ \left. + \frac{\partial(w^*+c)}{\xi^{*3} \partial \xi^*} \right] + \left[\varphi^* \rho_p + (1 - \varphi^*) \left\{ \rho_f (1 - \beta_T (v^* - v_w)) \right\} \right] g - \frac{\partial P^*}{\partial \xi^*} \\ + \mu \left[\frac{\partial^2(w^*+c)}{\partial \xi^{*2}} + \frac{\partial(w^*+c)}{\xi^* \partial \xi^*} + \frac{\partial^2(w^*+c)}{\partial \eta^{*2}} \right]. \end{aligned} \quad (14)$$

$$\begin{aligned} u^* \frac{\partial v^*}{\partial \xi^*} - c \frac{\partial v^*}{\partial \eta^*} + (w^*+c) \frac{\partial v^*}{\partial \eta^*} = \frac{k}{(\rho c)_f} \left(\frac{\partial^2 v^*}{\partial \xi^{*2}} + \frac{1}{\xi^*} \frac{\partial v^*}{\partial \xi^*} + \frac{\partial^2 v^*}{\partial \eta^{*2}} \right) + \frac{(\rho c)_p}{(\rho c)_f} \\ \left[D_b (\varphi_m - \varphi_w) \left\{ \frac{\partial \varphi^*}{\partial \xi^*} \frac{\partial v^*}{\partial \xi^*} + \frac{\partial \varphi^*}{\partial \eta^*} \frac{\partial v^*}{\partial \eta^*} \right\} + \frac{D_T (v_m - v_w)}{v_w} \left\{ \left(\frac{\partial v^*}{\partial \xi^*} \right)^2 + \left(\frac{\partial v^*}{\partial \eta^*} \right)^2 \right\} \right]. \end{aligned} \quad (15)$$

$$\begin{aligned} \left[u^* \frac{\partial \varphi^*}{\partial \xi^*} + w^* \frac{\partial \varphi^*}{\partial \eta^*} \right] = \frac{D_T}{v_w} \left(\frac{\partial^2 v^*}{\partial \xi^{*2}} + \frac{1}{\xi^*} \frac{\partial v^*}{\partial \xi^*} + \frac{\partial^2 v^*}{\partial \eta^{*2}} \right) - k_r^2 \left(\frac{v^*}{v_w} \right)^n (\varphi^* - \varphi_w) \exp\left(\frac{-E_a}{k v^*} \right) \\ + D_b \left(\frac{\partial^2 \varphi^*}{\partial \xi^{*2}} + \frac{1}{\xi^*} \frac{\partial \varphi^*}{\partial \xi^*} + \frac{\partial^2 \varphi^*}{\partial \eta^{*2}} \right). \end{aligned} \quad (16)$$

3. Results

Dealing with an unsteady peristaltic transport of couple stress fluid suspended with heated golden nano-sized particles ends up with a system of ordinary differential equations. These differential equations were mutually intermingled with each other, involving a nonlinear composition. Therefore, for such complex geometry, an exact solution was not possible. This means one has to turn to a numerical scheme suitable for tackling the said issue. In order to achieve the desired goal, first we

have to make the entire system a non-dimensional form, by using the following transformations along with Oberbeck-Boussinesq approximation and long wave length assumption:

$$\begin{aligned} \frac{\xi^*}{\xi_2} &= \bar{\xi}; \quad \frac{\eta^*}{\lambda} = \bar{\eta}; \quad \frac{u^*}{c \delta} = \bar{u}; \quad \frac{w^*}{c} = \bar{w}; \quad \frac{\xi_2}{\lambda} = \delta; \quad \frac{\xi_2^2 P^*}{c \lambda \mu} = \bar{P}; \quad \frac{(\rho c)_p}{(\rho c)_f} = \tau; \\ \frac{k}{(\rho c)_f} &= \alpha; \quad \sqrt{\frac{\mu}{\gamma_1}} \xi_2 = \gamma; \quad 1 + \bar{\epsilon} \cos(2\pi \bar{\eta}) = R_2; \quad E^* = \frac{E_a}{k v_w}; \\ \frac{\xi_2^2 (v_m - v_w) (1 - \varphi_w) g \rho_f \beta_T}{c \mu} &= G_r; \quad D_b (\varphi_m - \varphi_w) = N_b; \quad A^* = \frac{k_r^2}{D_b}; \\ \frac{v^* - v_w}{v_m - v_w} &= \bar{v}; \quad \frac{\varphi^* - \varphi_w}{\varphi_m - \varphi_w} = \bar{\varphi}; \quad \frac{D_T (v_m - v_w)}{v_w} = N_t; \quad \frac{d}{\xi_2} = \bar{\epsilon}; \\ \frac{\xi_2^2 (\varphi_m - \varphi_w) (\rho_p - \rho_f) g}{c \mu} &= B_r; \quad \frac{\xi_1}{\xi_2} = R_1; \quad \beta^* = \frac{(v_m - v_w)}{v_w}. \end{aligned} \quad (17)$$

Equations (13)–(16) in dimensionless form can be obtained as:

$$\frac{d\bar{P}}{d\bar{\eta}} = \frac{d^2\bar{w}}{d\bar{\xi}^2} + \frac{1}{\bar{\xi}} \frac{d\bar{w}}{d\bar{\xi}} - \frac{1}{\gamma^2} \left[\frac{d^4\bar{w}}{d\bar{\xi}^4} + \frac{2}{\bar{\xi}} \frac{d^3\bar{w}}{d\bar{\xi}^3} + \frac{d^2\bar{w}}{\bar{\xi}^2 d\bar{\xi}^2} + \frac{d\bar{w}}{\bar{\xi}^3 d\bar{\xi}} \right] + B_r \bar{\varphi} + G_r \bar{v}, \quad (18)$$

$$\alpha \left(\frac{\partial^2 \bar{v}}{\partial \bar{\xi}^2} + \frac{1}{\bar{\xi}} \frac{\partial \bar{v}}{\partial \bar{\xi}} \right) + \tau \left\{ N_b \left(\frac{\partial \bar{\varphi}}{\partial \bar{\xi}} \right) \left(\frac{\partial \bar{v}}{\partial \bar{\xi}} \right) + N_t \left(\frac{\partial \bar{v}}{\partial \bar{\xi}} \right)^2 \right\} = 0, \quad (19)$$

$$N_b \left(\frac{\partial^2 \bar{\varphi}}{\partial \bar{\xi}^2} + \frac{1}{\bar{\xi}} \frac{\partial \bar{\varphi}}{\partial \bar{\xi}} \right) + N_t \left(\frac{\partial^2 \bar{v}}{\partial \bar{\xi}^2} + \frac{1}{\bar{\xi}} \frac{\partial \bar{v}}{\partial \bar{\xi}} \right) - \{ A^* (\beta^* \bar{v} + 1)^n N_b \} \bar{\varphi} \exp \left(\frac{-E^*}{\beta^* \bar{v} + 1} \right) = 0. \quad (20)$$

Also, the corresponding boundary conditions in dimensionless form are as follows.

At the rigid wall:

$$\left. \begin{aligned} (i). \bar{w}(\bar{\xi}) &= -1, \\ (ii). \bar{v}(\bar{\xi}) &= 1, \\ (iii). \bar{\varphi}(\bar{\xi}) &= 1. \end{aligned} \right\}; \text{ When } \bar{\xi} = R_1. \quad (21)$$

At the flexible wall:

$$\left. \begin{aligned} (i). \bar{w}(\bar{\xi}) &= -1, \\ (ii). \bar{v}(\bar{\xi}) &= 0, \\ (iii). \bar{\varphi}(\bar{\xi}) &= 0. \end{aligned} \right\}; \text{ When } \bar{\xi} = R_2. \quad (22)$$

Finally, to obtain reliable solutions of Equations (18)–(20) subject to corresponding boundary conditions given in Equations (21) and (22), the most efficient numerical approach, Keller-box scheme, [32] is utilized. This method is much faster and more flexible to use as compared to other methods. It has been extensively used and tested on boundary layer flows. By means of said method, the solution can be attained by using four steps: (i) First reduce the system of equations to a first order system; (ii) then write the difference equations by means of central differences; (iii) now linearize the resulting nonlinear equation by Newton's method, if needed; and (iv) finally the block-tridiagonal-elimination technique is used to solve the linear system.

4. Discussion

This graphical section is relevant to the effectively contributing parameters, which influence axial velocity of couple stress fluid, temperature of nanofluid, and concentration of nano sized Hafnium particles, respectively. The involved parameters have a greater impression on the flow, namely, couple stress parameter γ , Brownian motion N_b and thermophoresis parameters N_t , thermophoresis diffusion G_r , and Brownian parameter B_r emerging due to the presence of heat and metallic particles. Moreover, a modified Arrhenius mathematical term yields some additional parameters, such as reaction rate A^* , activation energy E^* , temperature difference parameter β^* , and the fitted rate constant n , assuming the contribution of peristaltic pressure to be constant. To make this more systematic, the main portion is further divided into four subsections.

4.1. Axial Velocity

Axial velocity is spotted in Figures 2–4 for couple stress parameter, Brownian diffusion constant, and Grashof number. Axial velocity, as shown in Figure 2, accelerates in response to an increases in couple stress parameter. This is mainly due to the decrease in friction, which arises from the particle (i.e., base-fluid particles) additives, which constitute a size-dependent effect in couple stress fluids. In addition to the preceding remark, the rotational field of fluid particles is minimal as well. The peristaltic motion of outer walls of the tube also contributes by rapidly pushing the fluid in the axial direction, as B_r gets numerically varied in Figure 3. Figure 4 displays a different picture of the velocity of the fluid for the case of thermophoresis diffusion constant. The diagram basically describes the influence of buoyancy in terms of Grashof number Gr . As one can see from Equation (17), the buoyancy effects are mainly due to gravity and temperature difference. Therefore, increase in Gr attenuates the fluid's momentum by aggravating buoyant force. This brings a vivid decline in the velocity of the fluid. Furthermore, the relation defining Gr suggests that if $Gr > 0$, then this physically describes the heating of the nanofluid, while a reverse case can be expected for $Gr < 0$.

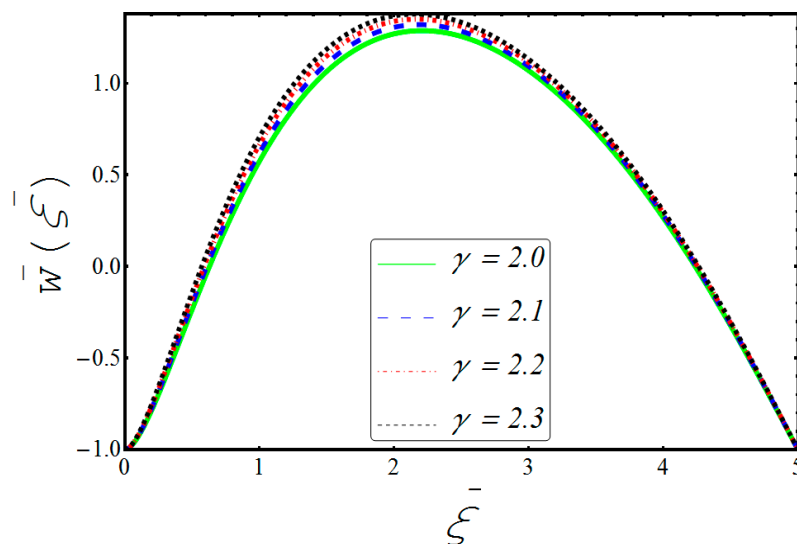


Figure 2. Axial velocity influenced by γ .

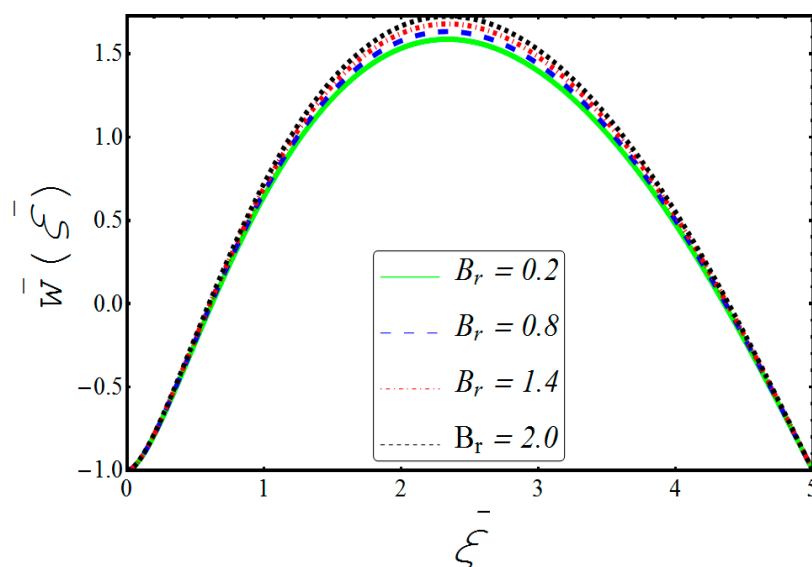


Figure 3. Axial velocity influenced by B_r .

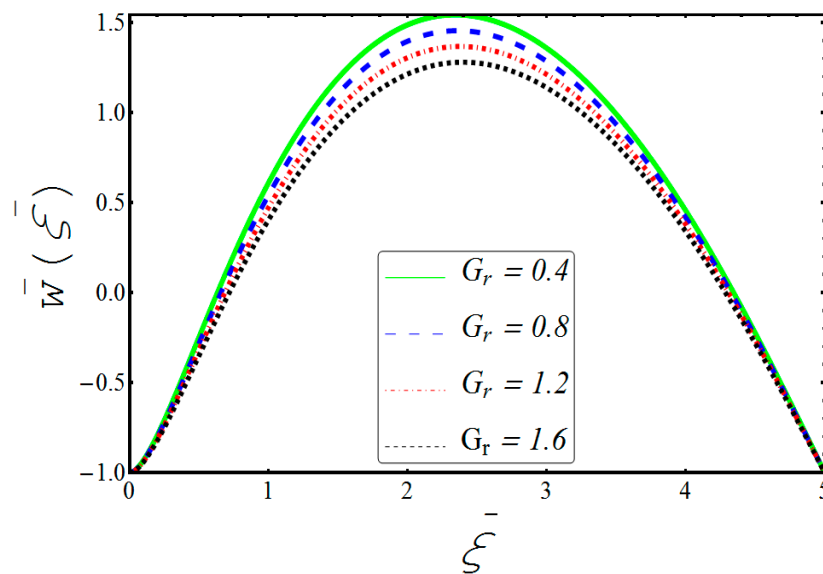


Figure 4. Axial velocity influenced by G_r .

4.2. Thermal Distribution

The temperature distribution of the nanofluid in the presence of additional chemical reaction and activation energy are portrayed in Figures 5 and 6. The variation of the Brownian motion parameter has noticeable effects on the nanofluid temperature, as the Brownian motion is generated due the collision of nanoparticles, driving the particles to a random motion. The collision of the particles, whether mutual or with the fluid molecules, is enhanced by the inward contraction of the flexible walls. Due to this factor Brownian motion parameter, N_b accumulates some additional thermal energy in the fluid, as shown in Figure 5. The nanoparticles were further thermally charged by the increase in N_t . It is important to keep in mind that the thermophoresis forces become stronger in the response of larger values of N_t , which finally result in higher temperature, as seen in Figure 6. Sometimes, such variations are credited to the thermal boundary layer thickness as well. Obviously, this increase in fluid temperature is due to increase in the random motion of nanoparticles when the above-mentioned parameters are increased.

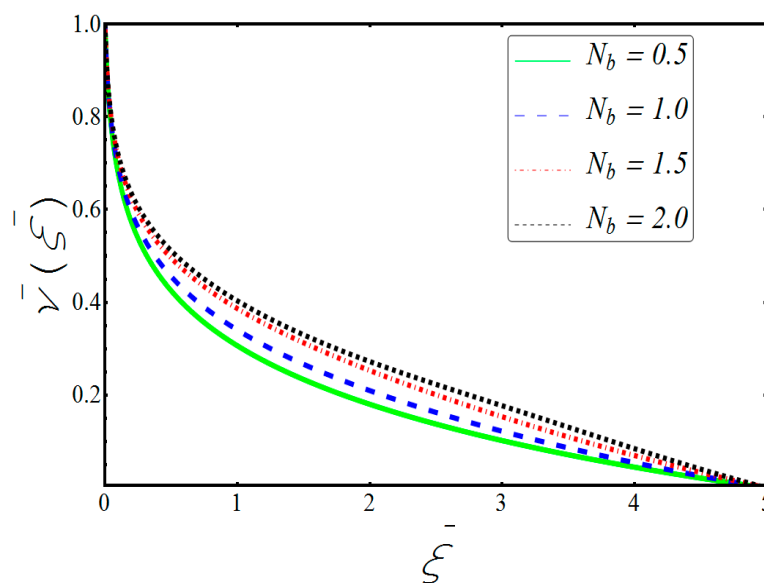


Figure 5. Temperature influenced by N_b .

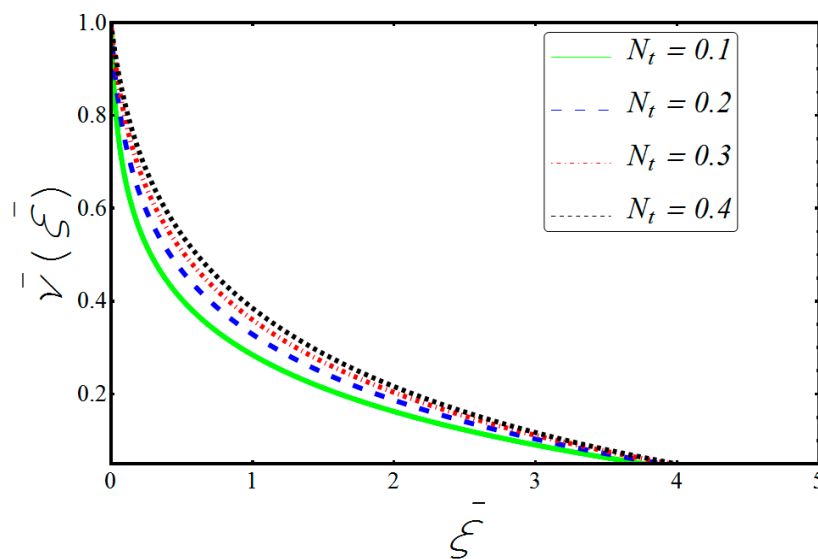


Figure 6. Temperature influenced by N_t .

4.3. Nanoparticle Concentration Profile

The concentration of golden particles is observed in Figures 7 and 8, when the Brownian motion parameter and thermophoresis parameter, respectively, are given higher numeric values. The random motion of the nanoparticles is seen to be faster in response to increase in the values of said parameters, which makes diffusion of nanoparticles rapid and fast. Therefore, rising curves show an increase in the concentration of nanoparticles. Moreover, this contribution of Brownian motion identifies the quick movement of hotter gold particle, from the region of higher temperature to lower temperature. The thermophoresis forces also bring positive effects on the golden particles by making the concentration strong against the higher numerical variation in N_t , as is noticeable in Figure 8. With the same trend of influence, an onward surge of activation energy again gives a rise to the golden solution. One can see in Figure 9 that the boundary layer thickness of the particles gets depreciated when E_a is further motivated to transport the required drug or medicine to the desired target. The Arrhenius equation, which gives the mathematical description of the introduction of activation energy into any system, clearly reveals that the reduction in heat and acceleration of E_a returns a low reaction rate constant. In the process, this slows down the chemical reaction and results in higher concentration of the particles, which confirms the accumulation of gold nanoparticles at the location of the malign tissue or organ to cured. Finally, the surge in concentration of gold particles is evidenced by the decline in Figures 10–12. The temperature difference ratio brings a remarkable decline in concentration of the heated nanoparticles. As the difference between the ambient fluid temperature and wall temperature widens, the concentration boundary layer thickness expands. This thickness resists the increase in particle concentration displayed in Figure 10. Similarly, retardation can be witnessed for reaction rate and fitted rate constant. It can be conceived that the rise in these parameters and constants sharpens the chemical reaction, which motivates the concentration gradient at the wall of the inner tube. Hence, a vivid reduction in the concentration of the particles occurs, as is seen in Figures 11 and 12).

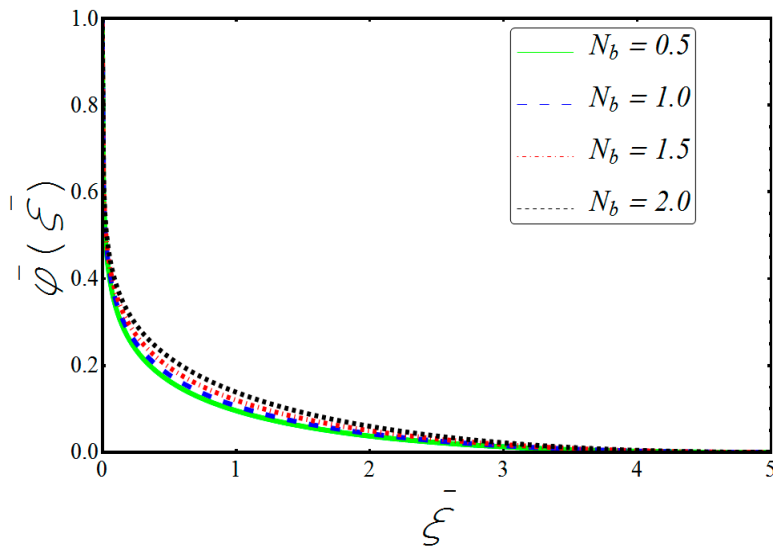


Figure 7. Concentration under the influence of N_b .

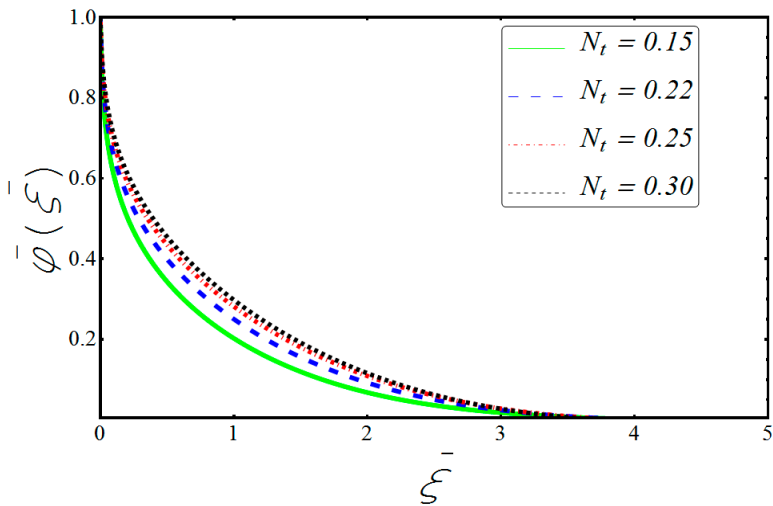


Figure 8. Concentration under the influence of N_t .

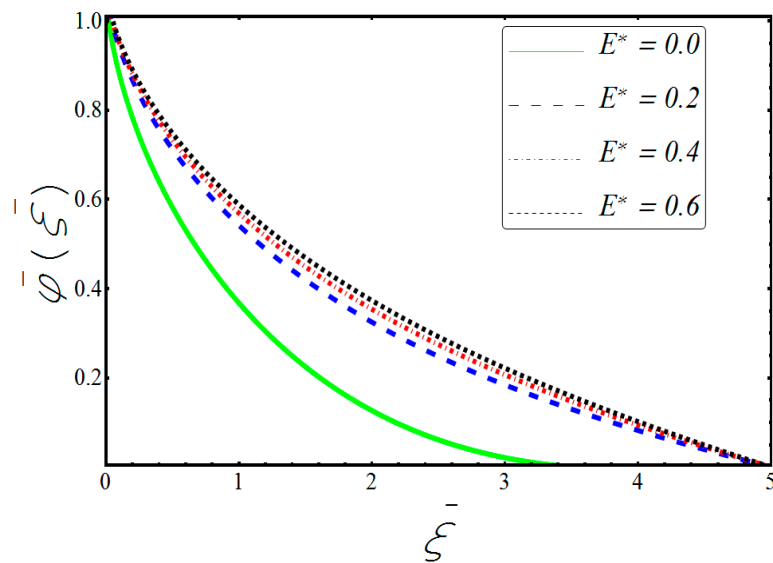


Figure 9. Concentration under the influence of E^* .

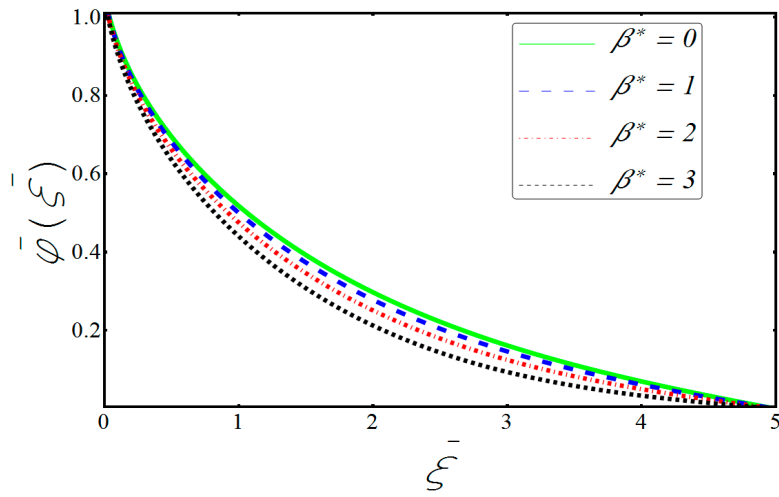


Figure 10. Concentration under the influence of β^* .

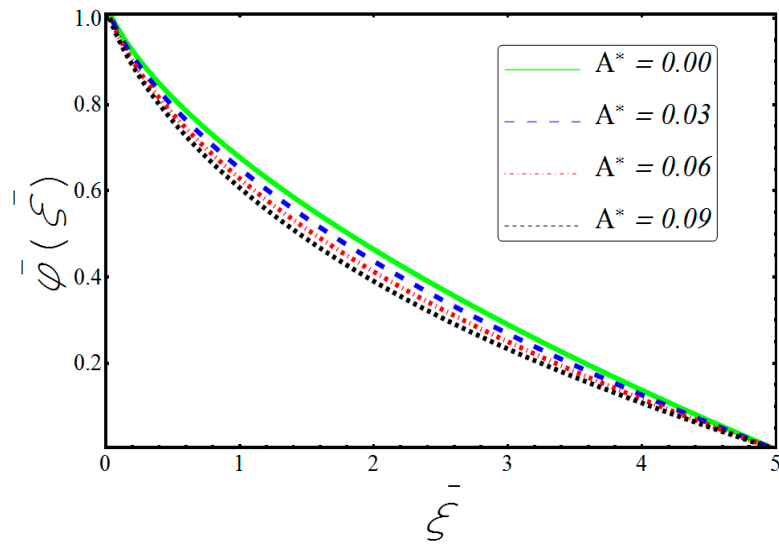


Figure 11. Concentration under the influence of A^* .

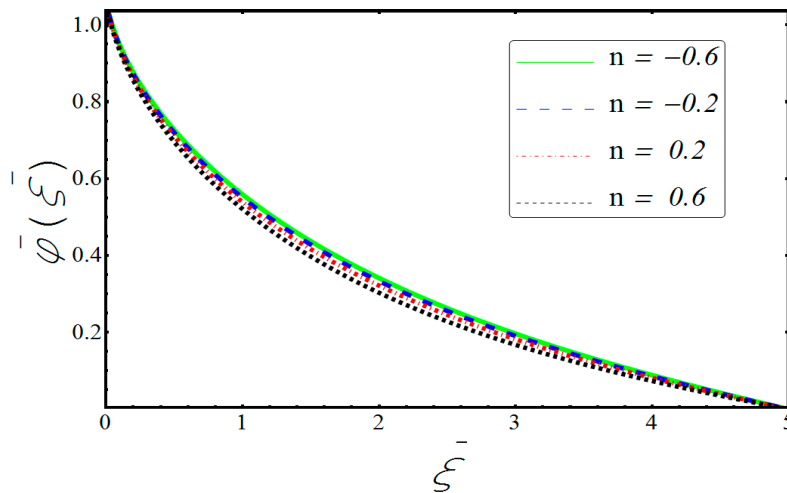


Figure 12. Concentration under the influence of n .

4.4. Trapping Phenomenon/ Streamline Configuration

Finally, the most significant phenomena relevant to any peristaltic motion in a living organism is known as “Trapping”. Essentially, this is the appearance of a round closed bolus, which is identified as the hallow cavity, transporting the required medication to the desired tissues or organs, as shown in Figures 13–19. In Figures 13 and 14, one can easily notice that the fluids face less resistance when traveling through the coaxial space, as the contours reduce in size and configuration. In contrast, the couple stress fluid results in shrinking the streamlines and generates the circulating boluses, as depicted in Figure 15. Isotherms of the Brownian motion parameter keep binding closer together, which allows the bolus to expand, as established in Figures 16 and 17, whereas the thermophoresis parameter provides extra potential for isotherms to compress the bolus inwards. Hence, the bolus keeps getting smaller. In the last two graphs, contours are sketched in order to see how concentration is influenced by the reaction rate constant and thermophoresis parameter. One can see in Figure 18 that the bolus bulges out as the reaction rate constant gets stronger, whereas a reverse trend is observed for the thermophoresis parameter in Figure 19.

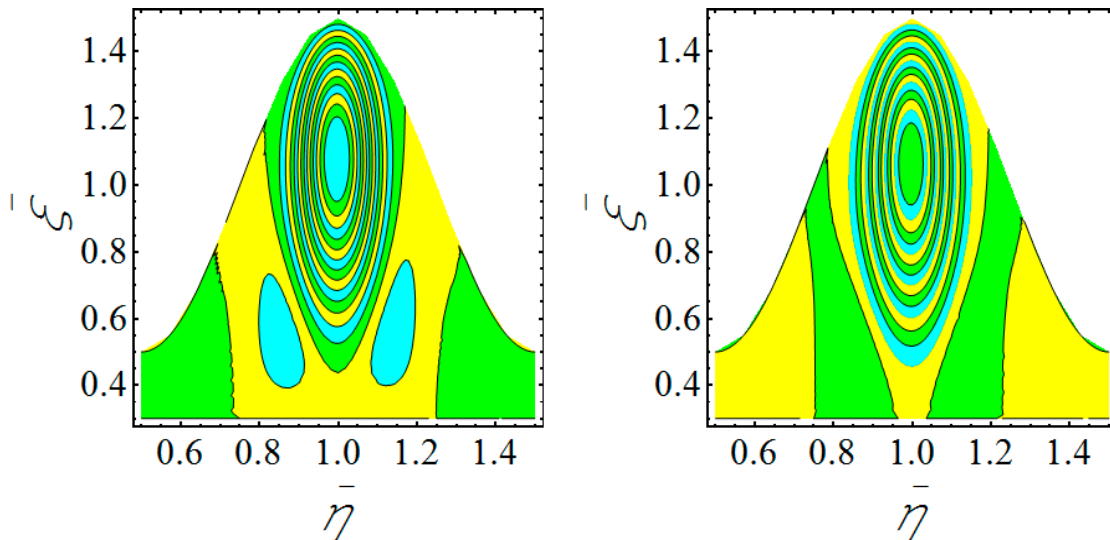


Figure 13. Stream lines for Brownian diffusion constant. (a): For $B_r = 0.2$; (b): For $B_r = 0.2$.

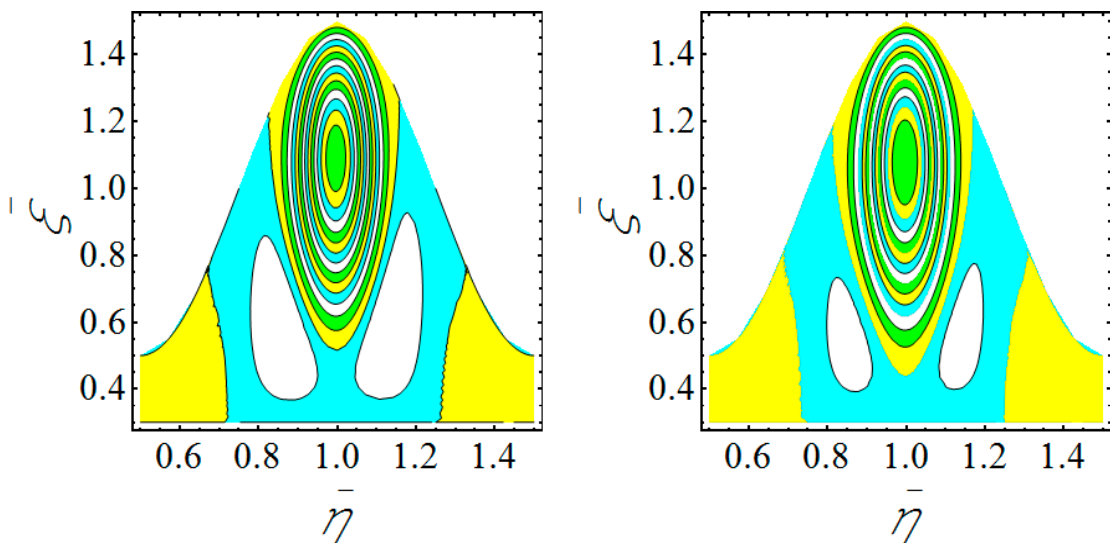


Figure 14. Stream lines for Grashof number. (a): For $G_r = 0.1$; (b): For $G_r = 0.3$.

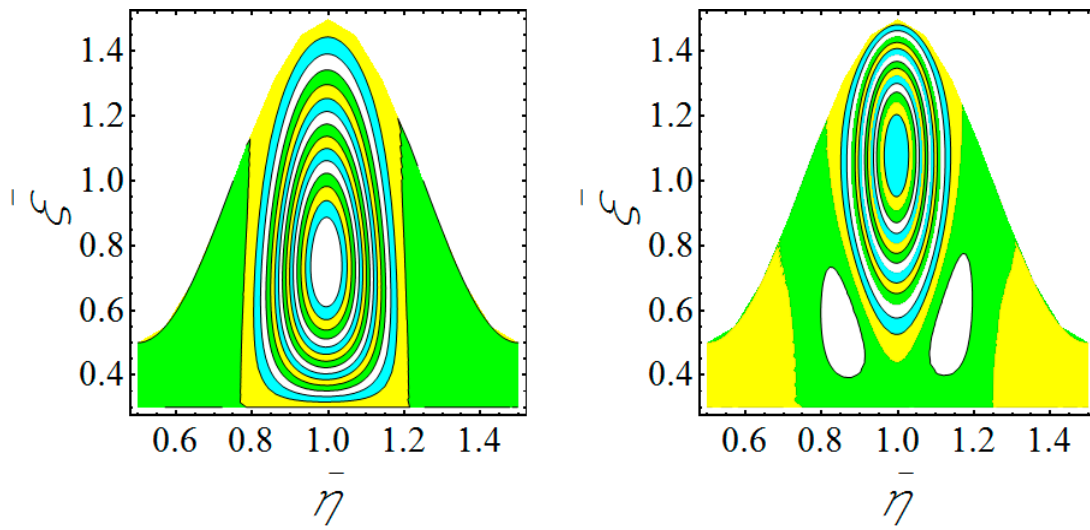


Figure 15. Stream lines for couple stress parameter. (a): For $\gamma = 1.0$; (b): For $\gamma = 2.0$.

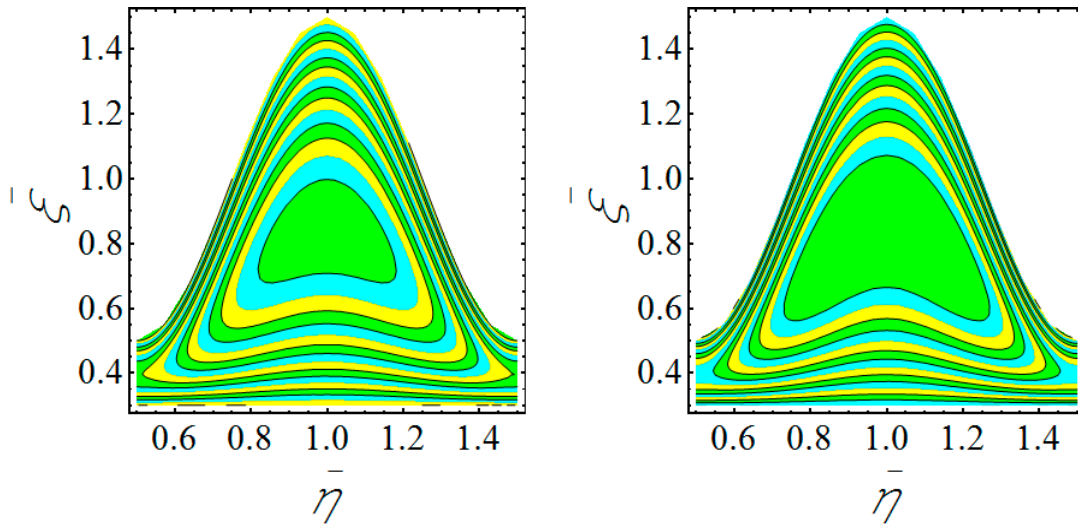


Figure 16. Isotherms for Brownian motion parameter. (a): For $N_b = 1.0$; (b): For $N_b = 1.5$.

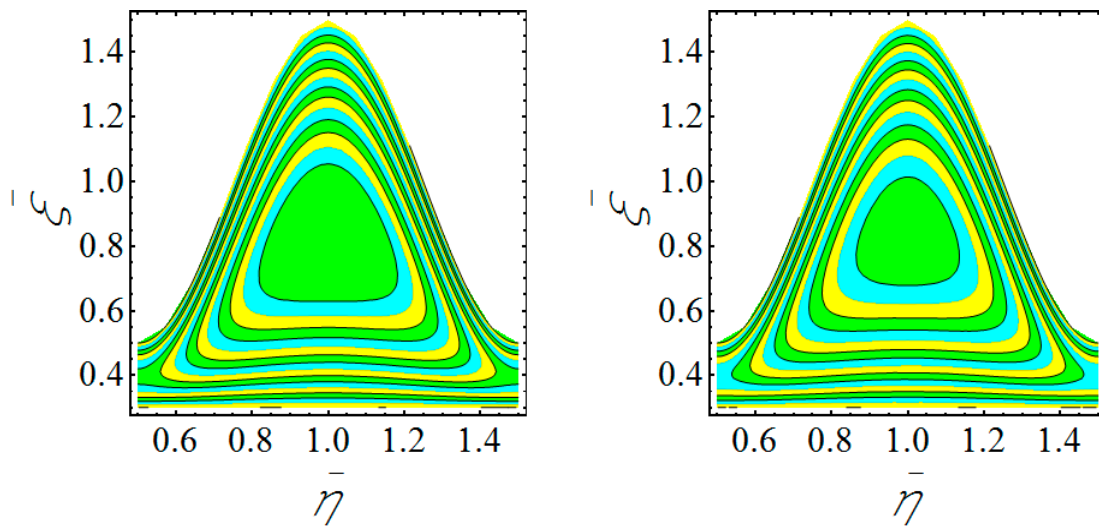


Figure 17. Isotherms for Thermophoresis parameter. (a): For $N_t = 0.2$; (b): For $N_t = 0.5$.

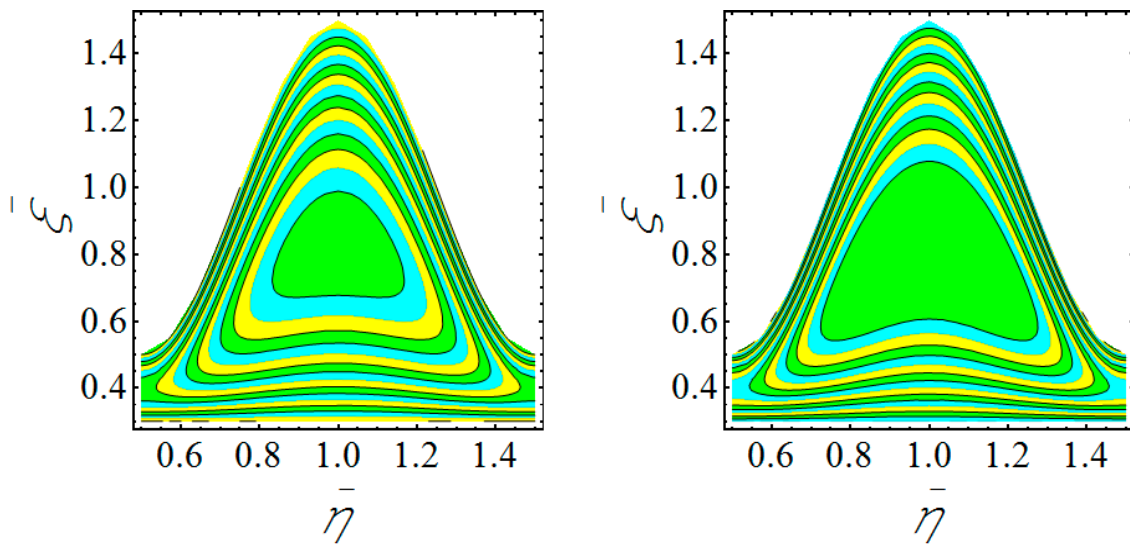


Figure 18. Contour plot for reaction rate constant. (a): For $A^* = 0.5$; (b): For $A^* = 1.0$.

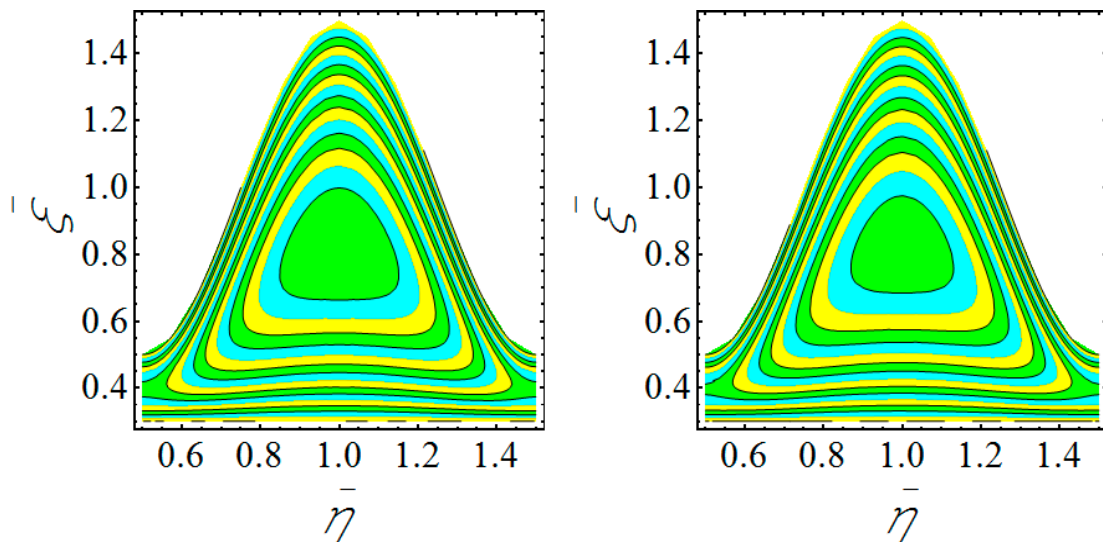


Figure 19. Contour plot for Thermophoresis parameter. (a): For $N_t = 0.2$; (b): For $N_t = 0.5$.

5. Conclusions

A numerical investigation is carried out for the peristaltic flow of nanofluids between the gap of two coaxial tubes with different configurations and structures. The nanofluid is composed of gold particles, while the couple stress fluid serves as the solvent. To enhance the mutual interaction of gold particles, or the interaction of molecules with the base fluid, additional effects of chemical reaction and activation energy have also been taken into consideration. The performed study reveals very informative results. Such results include that axial velocity is fully supported by the couple stress parameter and Brownian diffusion constant, in contrast to the Grashof number. The temperature of the nanofluid remains high for both involved parameters, which are thermophoresis and Brownian motion parameter. Looking at the graphs of concentrations of the metallic particles, it is inferred that activation energy, thermophoresis, and Brownian motion parameters cause an increase in the concentration of particles, whereas temperature ratio, reaction rate, and fitted rate constants do not support the increase. In the final portion of the graphical study, the number and size of the circulating boluses are depicted. One can easily notice that boluses get enlarged in response to the Brownian motion parameter, couples stress parameter, and reaction rate constant. However, a reverse trend

is observed for the Grashof number, thermophoresis parameter, and Brownian diffusion constant. The key finding can be summarized as:

- Strong buoyant force results in retarded axial velocity for the thermophoresis parameter.
- Peristaltic movement of the outer tube enhances the Brownian motion and raises the temperature of the nanofluid.
- Activation energy entering the process maximizes the concentration boundary layer thickness.
- The reaction rate constant increases concentration at the catheter, which decreases the concentration of nanoparticles.
- The thermophoresis parameter shrinks the size of the bolus by strengthening isotherms and closed paths of concentration lines.
- The couple stress parameter and reaction rate constant give freedom to the bolus to swell by binding the stream lines closer to each another.

Author Contributions: Supervision, R.E.; conceptualization, A.Z.; investigation, F.H.; methodology, A.A.

Funding: This research received no external funding.

Acknowledgments: R. Ellahi gratefully thanks Prof. Sadiq M. Sait, the Director Office of Research Chair Professors, King Fahd University of Petroleum and Minerals, Dhahran, Saudi Arabia, to honor him with the Chair Professor at KFUPM. F. Hussain is also HEC (Higher Education Commission Pakistan) to provide him the title of indigenous scholar for the pursuance of his Ph.D. studies.

Conflicts of Interest: The authors declare no conflict of interest.

Nomenclature

| | |
|-----------|--|
| V | Nanofluid velocity |
| G | Gravitational acceleration |
| u | Radial velocity Component (fixed frame) |
| w | Axial velocity component (Fixed frame) |
| u^* | Radial velocity component (wave frame) |
| w^* | Axial velocity component (Wave frame) |
| \bar{u} | Dimensionless radial velocity component |
| \bar{w} | Dimensionless lateral velocity component |
| d | Amplitude of peristaltic wave |
| t | Time |
| k_r | Rate of reaction |
| c | Propagating velocity of wave |
| N_t | Thermophoresis parameter |
| k | Thermal conductivity |
| N_b | Brownian motion parameter |
| G_r | Grashof number |
| D_t | Thermophoretic diffusion coefficient |
| D_b | Brownian motion coefficient |
| d | Amplitude of peristaltic wave |
| t | Time |
| R_2 | Dimensionless radius of outer tube |
| R_1 | Dimensionless radius of inner tube |
| P^* | Dimensional pressure |
| B_r | Brownian diffusion constant |
| A^* | Reaction rate constant |
| E^* | Activation energy (Dimensionless) |
| E_a | Activation energy (Dimensional) |
| n | Fitted rate constant |

Greek Symbols

| | |
|------------------|--|
| ζ | Radial direction of the flow (Fixed frame) |
| η | Axial direction of the flow (Fixed frame) |
| ζ^* | Radial direction of the flow (Wave frame) |
| η^* | Axial direction of the flow (Wave frame) |
| $\bar{\zeta}$ | Radial direction of the flow (Dimensionless) |
| $\bar{\eta}$ | Axial direction of the flow (Dimensionless) |
| ζ_1 | Radius of inner tube (Dimensional) |
| ζ_2 | Radius of outer tube (Dimensional) |
| $\vec{\varphi}$ | Nanoparticle concentration (Fixed frame) |
| \vec{v} | Nanofluid temperature (Fixed frame) |
| φ^* | Nanoparticle concentration (Wave frame) |
| v^* | Nanofluid temperature (Wave frame) |
| $\bar{\varphi}$ | Nanoparticle concentration (Dimensionless) |
| \bar{v} | Nanofluid temperature (Dimensionless) |
| γ_1 | Couple stress fluid's constant |
| γ | Couple stress parameter |
| τ | A ratio defined as $\frac{(\tilde{\rho}c)_f}{(\tilde{\rho}c)_p}$ |
| β^* | Temperature ratio |
| ρ_p | Density of nanoparticle at reference temperature |
| ρ_f | Density of nanofluid at reference temperature |
| $(\rho c)_f$ | Heat capacity of base fluid |
| $(\rho c)_p$ | Heat capacity of particle |
| μ | Dynamic Viscosity |
| ν | Kinematic viscosity |
| λ | Wavelength |
| α | Ratio defined as $\frac{k}{(\rho c)_f}$ |
| $\bar{\epsilon}$ | A constant ratio |
| β_T | Volumetric coefficient of expansion |
| φ_w | Reference concentration |
| v_w | Reference temperature |
| φ_m | Mass concentration |
| v_m | Fluid temperature |

Subscripts

| | |
|-----|------------|
| f | Base fluid |
| p | Particle |

References

1. Karimipour, A.; Orazio, A.D.; Shadloo, M.S. The effects of different nano particles of Al₂O₃ and Ag on the MHD nano fluid flow and heat transfer in a microchannel including slip velocity and temperature jump. *Physica E* **2017**, *86*, 146–153. [[CrossRef](#)]
2. Tripathi, D.; Beg, O.A. A study on peristaltic flow of nanofluids: Application in drug delivery systems. *Int. J. Heat Mass Transf.* **2014**, *70*, 61–70. [[CrossRef](#)]
3. Nabil, T.M.; El-dabe, N.T.M.; Moatimid, G.M.; Hassan, M.A.; Godh, W.A. Wall properties of peristaltic MHD Nanofluid flow through porous channel. *Fluid Mech. Res. Int.* **2018**, *2*, 19. [[CrossRef](#)]
4. Swarnalathamma, B.V.; Krishna, M.V. Peristaltic hemodynamic flow of couple stress fluid through a porous medium under the influence of magnetic field with slip effect. *AIP Conf. Proc.* **2016**, *1728*, 020603. [[CrossRef](#)]
5. Shit, G.C.; Roy, M. Hydromagnetic effect on inclined peristaltic flow of a couple stress fluid, Hydromagnetic effect on inclined peristaltic flow of a couple stress fluid. *Alex. Eng. J.* **2014**, *53*, 949–958. [[CrossRef](#)]
6. Jamalabadi, M.Y.A.; Daqiqshirazi, M.; Nasiri, H.; Safaei, M.R.; Nguyen, T.K. Modeling and analysis of biomagnetic blood Carreau fluid flow through a stenosis artery with magnetic heat transfer: A transient study. *PLoS ONE* **2018**, *13*, e0192138. [[CrossRef](#)]

7. Hosseini, S.M.; Safaei, M.R.; Goodarzi, M.; Alrashed, A.A.A.A.; Nguyen, T.K. New temperature, interfacial shell dependent dimensionless model for thermal conductivity of nanofluids. *Int. J. Heat Mass Transf.* **2017**, *114*, 207–210. [[CrossRef](#)]
8. Mekheimer, K.; Hasona, W.; Abo-Elkhair, R.E.; Zaher, A. Peristaltic blood flow with gold nanoparticles as a third grade nanofluid in catheter. *Appl. Cancer Ther. Phys. Lett. A* **2018**, *382*, 85–93.
9. Nasiri, H.; Jamalabadi, M.Y.A.; Sadeghi, R.; Safaei, M.R.; Nguyen, T.K.; Shadloo, M.S. A smoothed particle hydrodynamics approach for numerical simulation of nano-fluid flows. *J. Anal. Calorim.* **2018**, 1–9. [[CrossRef](#)]
10. Shadloo, M.S.; Kimiaefar, A. Application of homotopy perturbation method to find an analytical solution for magnetohydrodynamic flows of viscoelastic fluids in converging/diverging channels. *Proc. Mech. Eng. Part C J. Mech. Eng.* **2011**, *225*, 347–353. [[CrossRef](#)]
11. Safaei, M.R.; Ahmadi, G.; Goodarzi, M.S.; Shadloo, M.S.; Goshayeshi, H.R.; Dahari, M. Heat transfer and pressure drop in fully developed turbulent flows of graphene nanoplatelets–silver/water nanofluids. *Fluids* **2016**, *1*, 20. [[CrossRef](#)]
12. Mohyud-Din, S.T.; Khan, U.; Ahmed, N.; Hassan, S.M. Magnetohydrodynamic flow and heat transfer of nanofluids in stretchable convergent/divergent channels. *Appl. Sci.* **2015**, *5*, 1639–1664. [[CrossRef](#)]
13. Chamkha, A.J.; Selimefendigil, F. Forced convection of pulsating nanofluid flow over a backward facing step with various particle shapes. *Energies* **2018**, *11*, 3068. [[CrossRef](#)]
14. Xu, Z.; Kleinstreuer, C. Direct nano-drug delivery for tumor targeting subject to shear-augmented diffusion in blood flow. *Med. Biol. Eng. Comput.* **2018**, *56*, 1949–1958. [[CrossRef](#)] [[PubMed](#)]
15. Rashidi, M.M.; Nasiri, M.; Shadloo, M.S.; Yang, Z. Entropy generation in a circular tube heat exchanger using nanofluids: Effects of different modeling approaches. *Heat Transf. Eng.* **2017**, *38*, 853–866. [[CrossRef](#)]
16. Jamalabadi, M.Y.A.; Safaei, M.R.; Alrashed, A.A.A.A.; Nguyen, T.K.; Filho, E.P.B. Entropy generation in thermal radiative loading of structures with distinct heaters. *Entropy* **2017**, *19*, 506. [[CrossRef](#)]
17. Sadiq, M.A. MHD stagnation point flow of nanofluid on a plate with anisotropic slip. *Symmetry* **2019**, *11*, 132. [[CrossRef](#)]
18. Jawad, M.; Shah, Z.; Islam, S.; Majdoubi, J.; Tlili, I.; Khan, W.; Khan, I. Impact of nonlinear thermal radiation and the viscous dissipation effect on the unsteady three-dimensional rotating flow of single-wall carbon nanotubes with aqueous suspensions. *Symmetry* **2019**, *11*, 207. [[CrossRef](#)]
19. Akbarzadeh, O.; Zabidi, N.A.M.; Wahab, Y.A.; Hamizi, N.A.; Chowdhury, Z.Z.; Merican, Z.M.A.; Rahman, M.A.; Akhter, S.; Rasouli, E.; Johan, M.R. Effect of cobalt catalyst confinement in carbon nanotubes support on fischer-tropsch synthesis performance. *Symmetry* **2018**, *10*, 572. [[CrossRef](#)]
20. Mustafa, M.; Khan, J.A.; Hayat, T.; Alsaedi, A. Buoyancy effects on the MHD nanofluid flow past a vertical surface with chemical reaction and activation energy. *Int. J. Heat Mass Transf.* **2017**, *108*, 1340–1346. [[CrossRef](#)]
21. Xu, H.; Fan, T.; Pop, I. Analysis of mixed convection flow of a nanofluid in a vertical channel with the Buongiorno mathematical model. *Int. Commun. Heat Mass Transf.* **2013**, *44*, 15–22. [[CrossRef](#)]
22. Sheikholeslami, M.; Bhatti, M.M. Active method for nanofluid heat transfer enhancement by means of EHD. *Int. J. Heat Mass Transf.* **2017**, *109*, 115–122. [[CrossRef](#)]
23. Bhatti, M.M.; Rashidi, M.M. Effects of thermo-diffusion and thermal radiation on Williamson nanofluid over a porous shrinking/stretching sheet. *J. Mol. Liq.* **2016**, *221*, 567–573. [[CrossRef](#)]
24. Marin, M. An approach of a heat-flux dependent theory for micropolar porous media. *Meccanica* **2016**, *51*, 127–1133. [[CrossRef](#)]
25. Rashidi, S.; Esfahani, J.A.; Ellahi, R. Convective heat transfer and particle motion in an obstructed duct with two side by side obstacles by means of DPM model. *Appl. Sci.* **2017**, *7*, 431. [[CrossRef](#)]
26. Zeeshan, A.; Ijaz, N.; Abbas, T.; Ellahi, R. The sustainable characteristic of Bio-bi-phase flow of peristaltic transport of MHD Jeffery fluid in human body. *Sustainability* **2018**, *10*, 2671. [[CrossRef](#)]
27. Hussain, F.; Ellahi, R.; Zeeshan, A. Mathematical models of electro magnetohydrodynamic multiphase flows synthesis with nanosized hafnium particles. *Appl. Sci.* **2018**, *8*, 275. [[CrossRef](#)]
28. Haq, R.U.; Soomro, F.A.; Hammouch, Z.; Rehman, S. Heat exchange within the partially heated C-shape cavity filled with the water based SWCNTs. *Int. J. Heat Mass Transf.* **2018**, *127*, 506–514. [[CrossRef](#)]
29. Kumar, R.V.M.S.S.K.; Kumar, G.V.; Raju, C.S.K.; Shehzad, S.A.; Varma, S.V.K. Analysis of Arrhenius activation energy in magnetohydrodynamic Carreau fluid flow through improved theory of heat diffusion and binary chemical reaction. *J. Phys. Commun.* **2018**, *2*, 35–49. [[CrossRef](#)]

30. Anuradha, S.; Yegammai, M. MHD radiative boundary layer flow of nanofluid past a vertical plate with effects of binary chemical reaction and activation energy. *J. Pure Appl. Math.* **2017**, *13*, 6377–6392.
31. Pal, D.; Talukdar, B. Perturbation analysis of unsteady magnetohydrodynamic convective heat and mass transfer in a boundary layer slip flow past a vertical permeable plate with thermal radiation and chemical reaction. *Commun. Nonlinear Sci. Numer. Simul.* **2010**, *15*, 1813–1830. [[CrossRef](#)]
32. Hossain, A., Md.; Subba, R.; Gorla, R. Natural convection flow of non-Newtonian power-law fluid from a slotted vertical isothermal surface. *Int. J. Numer. Methods Heat Fluid Flow* **2009**, *19*, 835–846. [[CrossRef](#)]



© 2019 by the authors. Licensee MDPI, Basel, Switzerland. This article is an open access article distributed under the terms and conditions of the Creative Commons Attribution (CC BY) license (<http://creativecommons.org/licenses/by/4.0/>).